LncRNA H19 promotes vascular inflammation and abdominal aortic aneurysm formation by functioning as a competing endogenous RNA

Yili Sun[a,1], Lintao Zhong[a,1], Xiang He[a], Shifei Wang[a], Yanxian Lai[a], Weilan Wu[a], Haoyu Song[a], Yijin Chen[a], Yang Yang[a], Wangjun Liao[b], Yulin Liao[a], Jianping Bin[a,*]

[a] State Key Laboratory of Organ Failure Research, Department of Cardiology, Nanfang Hospital, Southern Medical University, Guangzhou 510515, China
[b] Department of Oncology, Nanfang Hospital, Southern Medical University, Guangzhou 510515, China

ABSTRACT

Abdominal aortic aneurysm (AAA) is accepted as a chronic vascular inflammatory disease. However, how the inflammatory response is regulated during AAA formation is not fully understood. This study was undertaken to determine whether the long noncoding RNA (lncRNA) H19 (H19) promotes AAA formation by enhancing aortic inflammation. qRT-PCR detected the upregulation of H19 in human and mouse AAA tissue samples. Co-staining for H19 and the macrophage marker MAC-2 showed that H19 was located in vascular smooth muscle cells (VSMCs) and infiltrating aortic macrophages. In vivo overexpression of H19 increased vascular inflammation and induced AAA formation, which was supported by exacerbated aortic morphology, maximum aortic diameter values, elastin degradation, expression of interleukin-6 (IL-6) and macrophage chemoattractant protein-1 (MCP-1), and macrophage infiltration. H19 suppression resulted in the opposite effects. A rescue experiment indicated that IL-6 neutralization significantly mitigated the aortic inflammation and AAA formation evoked by H19 overexpression. Luciferase reporter assays and ex vivo experiments using VSMCs and macrophages confirmed that H19 induced aneurysm formation in part via endogenous competition with the let-7a microRNA to induce the transcription of its target gene, IL-6. This mechanism was further validated by in vivo experiments using a mutant H19 that could not effectively bind let-7a. Collectively, our study revealed a pathogenic H19/let-7a/IL-6 inflammatory pathway in AAA formation, which offers a new potential therapeutic strategy for AAA.

1. Introduction

Abdominal aortic aneurysm (AAA) is an aberrantly enlarged aorta; although the morbidity of this condition is rising, it is generally asymptomatic, and rupture is often unexpected and highly lethal [1]. AAA is considered a chronic vascular inflammatory disease and is characterized by, mediated by, and induced by monocyte/macrophage cell infiltration into the aortic layers, accompanied by a range of excessive proinflammatory molecules and chemokines, such as interleukin-6 (IL-6), nuclear factor-kappa B (NF-κB), and monocyte chemoattractant protein-1 (MCP-1), all of which are well-established contributors to AAA [2–5]. However, how the inflammatory response is regulated during AAA formation is not fully understood.

Long noncoding RNAs (lncRNAs) are versatile and powerful regulators during protein-coding gene transcription, epigenetic modification, and translation in diverse biological and pathological contexts,

making lncRNA a high-profile potential therapeutic target [6]. Currently, emerging evidence proposes that lncRNAs are crucial mediators in inflammation and vascular function. Knockdown of the lncRNA Mirt1 mitigates myocardial infarction injury, presumably by reducing inflammatory cell infiltration [7]. Reduction in the level of lncRNA RNCR3 aggravates hypercholesterolemia and inflammatory factor release, followed by accelerated atherosclerosis formation [8]. Given the chronic vascular inflammation that characterizes AAA and the promising function of lncRNAs in inflammatory processes, it is possible that certain lncRNAs act as regulators of inflammatory processes during AAA formation.

LncRNA H19 (H19) is a developmentally regulated RNA whose expression is retained only in the adult heart and skeletal muscle. The re-expression of H19 in other tissues is closely related to inflammatory disorders [9,10]. Increased H19 expression accelerates atherosclerosis by activating inflammatory pathways, while H19 silencing suppresses

Fig. 1. H19 is re-expressed in human aortic aneurysm samples and Ang II- and CaCl$_2$-induced mouse aortas.
A to C, qRT-PCR results for human aortic expression levels of IL-6 (A), MCP-1 (B) and H19 (C) ($n = 5$). Male ApoE$^{-/-}$ mice were infused with Ang II (1 μg/kg/min) or an equal amount of normal saline for 28 days. D, qRT-PCR analysis of mouse aortic H19 expression ($n = 5$). E, Co-staining combining in situ hybridization of H19 and immunofluorescent staining of macrophages (MAC-2) in serial sections of aorta samples ($n = 5$). Suprarenal aortas of male C57BL/6 J mice were treated with CaCl$_2$ gauze or normal saline gauze for 15 min. Detection was performed 3 weeks later. F, qRT-PCR results for mouse aortic H19 levels (n = 5). G, Co-staining combining in situ hybridization of H19 and immunofluorescent staining of macrophages (MAC-2) (n = 5). Data are presented as the mean ± SD of three independent experiments. $^{**}P < .01$.
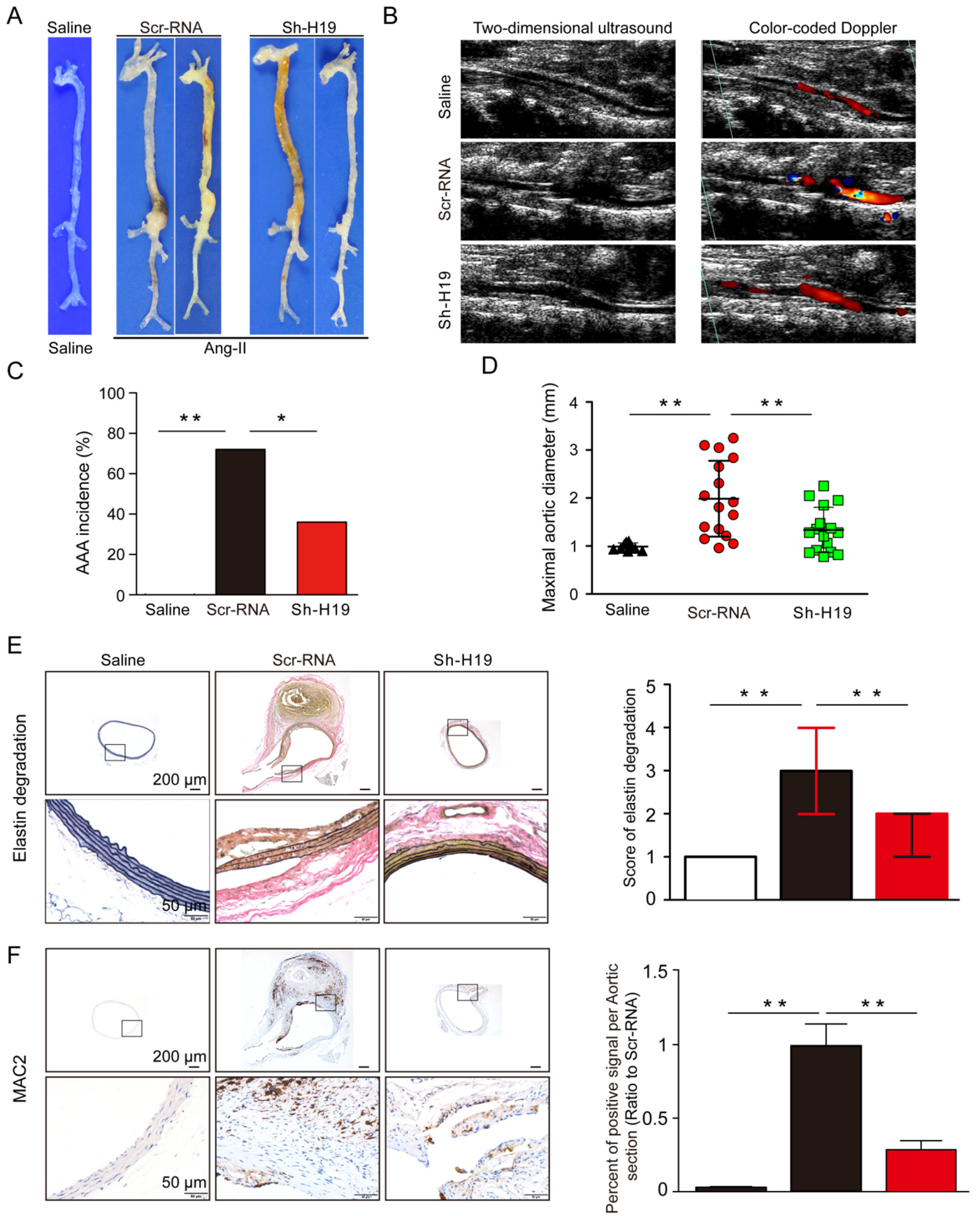
(caption on next page)

Fig. 2. H19 reduction prevents AAA formation in Ang II-treated ApoE$^{-/-}$ mice.

Male ApoE$^{-/-}$ mice were transfected with Scr-RNA or Sh-H19 ($n = 25$ per group). Thirty days later, they were infused with Ang II for an additional 28 days. Saline, male ApoE$^{-/-}$ mice with sham normal saline injection were infused with an equal amount of normal saline for 28 days ($n = 10$). (A) Representative images of macroscopic features of the aorta. (B) Two-dimensional ultrasound and color-coded Doppler imaging of the aorta. (C) Statistical analysis of AAA incidence ($n = 25$ per group). (D) Maximal aortic diameter of the abdominal region ($n = 16$ per group). (E) Representative elastin staining and elastin degradation scores in aortas. Images show the location where the most severe elastin degradation occurred ($n = 15$ per group; scale bars: upper 200 μm, lower 50 μm; magnified images). (F) Representative immunofluorescence staining of aortic MAC-2 ($n = 4$ per group; scale bars: upper 200 μm, lower 50 μm; magnified photographs). The data are presented as the mean ± SD or as the median and IQR (for elastin degradation score). $^*P < .05$, $^{**}P < .01$.

ex vivo adipogenesis and inflammatory responses induced by oxidized low-density lipoprotein (ox-LDL) treatment [11]. In an inflammatory cholangiocarcinoma model, a high level of H19 enhanced IL-6 expression and exaggerated cholangiocarcinoma cell migration [12]. Additionally, aortic H19 upregulation can be induced by hyperhomocysteinemia, a nonhomeostatic state that is strongly associated with AAA formation and that aggravates inflammation and atherosclerosis in ApoE$^{-/-}$ mice [13]. These findings imply the potential yet unexplored involvement of H19 in AAA formation via the modification of aortic inflammation. Inspiringly, a recent work demonstrated that H19 induces AAA formation; however, the authors proposed that H19 induced this effect by promoting apoptosis in vascular smooth muscle cells (VSMCs) [14]. Whether H19 can affect AAA formation by enhancing inflammatory responses awaits exploration.

In this work, we hypothesized that H19 is re-expressed during AAA and promotes AAA formation by augmenting vascular inflammatory responses. We detected the H19 content in human and mouse AAA. By inducing the overexpression and downregulation of H19 in two accepted AAA models, we explored the effects of H19 on AAA development. Moreover, the associated mechanism was investigated ex vivo and in vivo to determine whether H19 functions through a competing endogenous RNA (ceRNA) mechanism to reduce microRNA let-7a bioavailability and induce the transcription of the let-7a target gene IL-6.

2. Materials and methods

2.1. Human AAA samples

All protocols using human aortic samples were approved by the Research Ethics Committees of Zhongshan People's Hospital, Sun Yat-sen Hospital and Guangzhou General Hospital of Guangzhou Military Region. AAA diagnosis was confirmed by computed tomography angiography before the operation. AAA samples and adjacent normal aortic tissues were obtained from 5 patients undergoing open surgical repair in the above hospitals. All aorta samples were immediately frozen in liquid nitrogen and stored at −80 °C until RNA extraction was performed.

2.2. Experimental animals

All animal experiments complied with the guidelines approved by the Institutional Animal Care and Use Committee of Southern Medical University. All animal care followed the Guidelines for the Care and Use of Laboratory Animals (NIH Publication, 8th Edition, 2011). Male C57BL/6 J mice with normal lipid metabolism and male ApoE$^{-/-}$ mice on a C57BL/6 background were provided by the Laboratory Animal Center of Southern Medical University. All animals in the study were fed a normal mouse diet. The mice were raised under pathogen-free conditions with water available at a constant temperature of 22 °C with 60–65% humidity.

2.3. Angiotensin II infusion

This study used 10- to 12-week-old male C57BL/6 J mice and 12- to 16-week-old male ApoE$^{-/-}$ mice. After the mice were anesthetized

with an intraperitoneal injection of pentobarbital (40 mg/kg), an osmotic minipump (ALZET, Model 2004, DURECT Corporation, Cupertino, CA, USA) was subcutaneously implanted in the dorsum of the neck via a small incision. Ang II (A9525, Sigma) or normal saline (0.9% NaCl) was infused via the minipump at a rate of 1 μg/kg/min for 28 days [15].

2.4. CaCl$_2$ treatment

Male C57BL/6 J mice aged 8–12 weeks were anesthetized with an intraperitoneal injection of pentobarbital (40 mg/kg) and then subjected to laparotomy. The abdominal aorta segment between the renal arteries and the bifurcation of the iliac arteries was dissociated from the surrounding retroperitoneal tissues. A video microscope was used to assess the diameter of this aortic segment in triplicate. Then, the AAA model was induced by covering the aortic adventitia with cotton gauze carrying 0.5 mol/L CaCl$_2$ for 15 min. Normal saline (0.9% NaCl) was used for the sham operation in control mice. Then, 0.9% sterile saline was used to wash the aorta, and the incision was sutured. After 3 weeks, the mice were sacrificed and subjected to laparotomy for further assessment [16].

2.5. Aneurysm quantification

All surviving mice were ultimately sacrificed and cut open ventrally to confirm the formation of aortic aneurysm. Aneurysm quantification was applied in mice receiving Ang II or sham normal saline perfusion. Phosphate-buffered saline (PBS) (10 mL) was injected into the left cardiac ventricles and exited through a manual crevasse in the right atrium. Then, the aorta was exposed, the periadventitial tissue was scraped, and the aorta was photographed under a dissecting microscope. The suprarenal region of the abdominal aorta was identified as the segment below the last pair of intercostal arteries and above the right renal branch. The outer circumference of the most dilated portion of the abdominal aorta was regarded as the maximal abdominal aortic diameter and was measured using Image-Pro Plus (Media Cybernetics). We adopted the established human definition of AAA as a $> 50\%$ increase in the outer diameter of the aorta relative to that of control mice. Aortic rupture was defined when there were blood clots in the thoracic cavity (thoracic aortic rupture) or in the retroperitoneal cavity (abdominal aortic rupture). To consider tissue degradation, animals that died of aortic rupture were used only for calculating the mortality and rupture rates and were otherwise excluded from the analysis. The outer width of the aorta were measured as previously described [17]. Evaluation of aortic aneurysms was carried out by another investigator who was blinded to the experimental treatments.

2.6. Ultrasound imaging

Surviving mice 4 weeks after Ang II infusion or 3 weeks after CaCl$_2$ treatment were intraperitoneally anesthetized with pentobarbital (40 mg/kg) to perform two-dimensional ultrasound imaging and color-coded Doppler. A Sequoia ultrasound system with a linear array ultrasound transducer was used (15 L8-S, mechanical index, 0.17; frequency, 14 MHz; Siemens Medical Systems) [18].
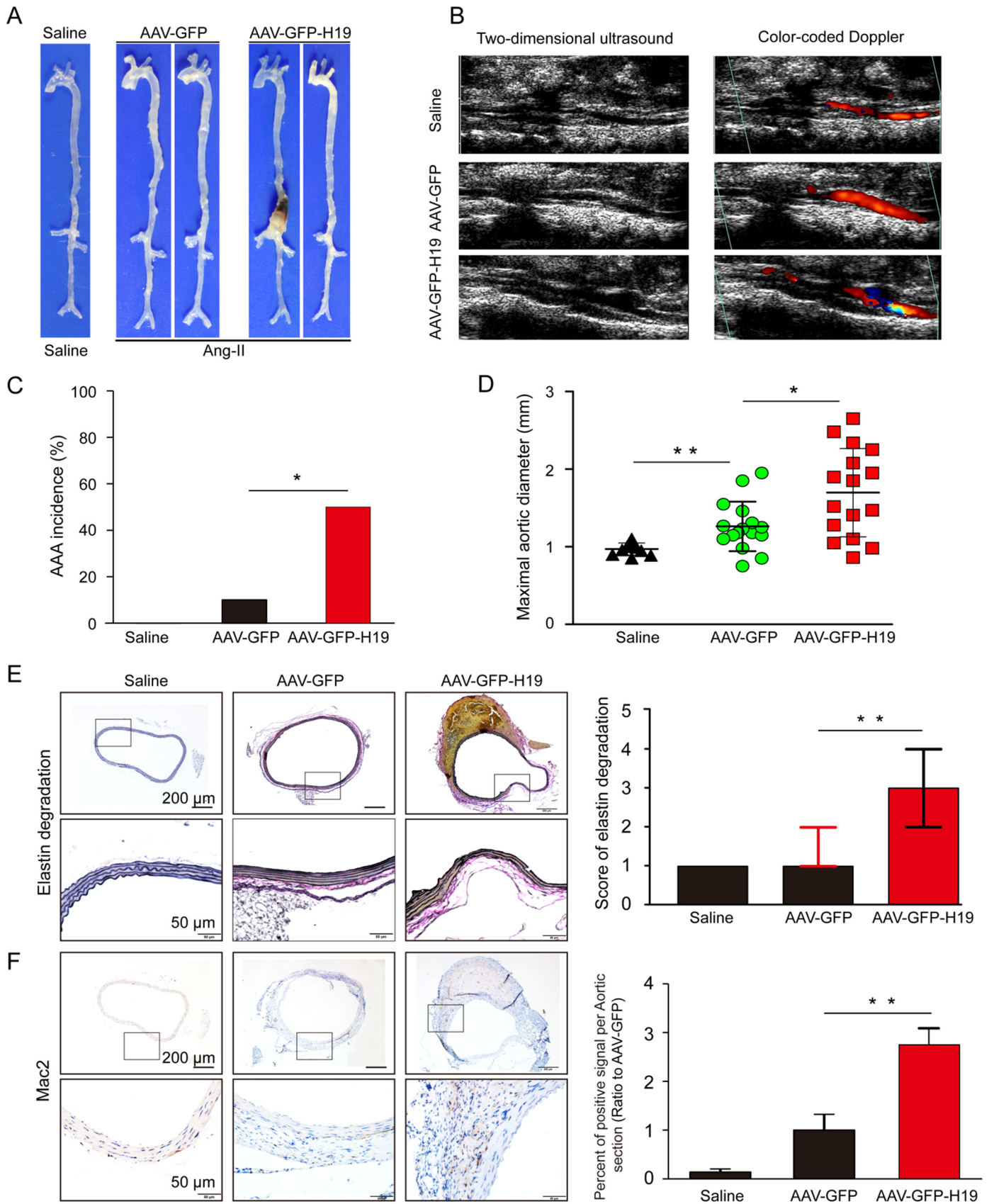
(caption on next page)

Fig. 3. H19 overexpression induces AAA formation in Ang II-treated C57BL/6 J mice.
Male C57BL/6J mice were transfected with AAV-GFP or AAV-GFP-H19 (n = 25 in each group). Thirty days later, they were infused with Ang II for an additional 28 days. The Saline group, male C57BL/6 J mice with sham normal saline injection, was infused with an equal amount of normal saline for 28 days (n = 10). (A) Representative images of macroscopic features of the aorta. (B) Two-dimensional ultrasound and color-coded Doppler imaging of the aorta. (C) Statistical analysis of AAA incidence in mice (n = 25 per group). (D) Maximal aortic diameter in the abdominal region (n = 16 per group). (E) Representative staining of elastin and elastin degradation scores in aortas (n = 15 per group). Photographs show the location where the most severe elastin degradation occurred (scale bars: upper 200 μm, lower 50 μm; magnified photographs). (F) Representative immunofluorescence staining and statistical analysis of aortic MAC-2 protein expression (n = 4; scale bars: upper 200 μm, lower 50 μm; magnified photographs). The data are presented as the mean ± SD or as the median and IQR (for elastin degradation score). $^*P$ < .05, $^{**}P$ < .01.

2.7. Blood pressure (BP) measurement

Systolic BP was monitored weekly in conscious mice throughout the study using a noninvasive tail-cuff system (BP-2010 series, Softron, Tokyo), as described in previous studies. The BP value measured 1 week prior to Ang II infusion was regarded as the baseline BP.

2.8. Histology and staining for elastin

A selected number of mice were sacrificed, and each whole mouse aorta was perfused with saline and fixed with 4% paraformaldehyde for 5 min. The segment from the ascending aorta to the entrance of both iliac arteries was isolated to perform macroscopic analysis. Then, the aorta was segmented to obtain the suprarenal abdominal section (for Ang II-induced AAA models) or the infrarenal abdominal section (for CaCl$_2$-induced AAA models). After harvesting, the samples were fixed for 24 h and embedded in paraffin. Histology was examined in cross-sections (5 μm each) at intervals of approximately 500 μm. At least 10 sections were analyzed per mouse. Paraffin sections were subjected to elastin van Gieson staining or used for immunostaining and in situ hybridization. A previously established standard for the elastin degradation score was adopted [19]: score 1, no elastin degradation with a well-organized elastin lamina; score 2, mild elastin degradation with some interruptions or breaks in the lamina; score 3, moderate elastin degradation with multiple interruptions or breaks in the lamina; and score 4, severe elastin fragmentation or loss or aortic rupture.

2.9. Cell culture

Mouse aortic VSMCs and mouse macrophages (Raw264.7) were purchased from Guangzhou Geneseed Biotech Co., Ltd. The cells were maintained in Dulbecco's modified Eagle's medium (DMEM) containing fetal bovine serum (10%), penicillin (100 U/mL) and streptomycin (100 μg/mL). Both cells were incubated at 37 °C in a humidified atmosphere containing 5% CO$_2$.

2.10. Transfection with adeno-associated viruses (AAVs)

AAV serotype-9, which can transfect the vasculature and adult aorta, was used in this study [20]. A specific duplex small interfering RNA (siRNA) against H19, Sh-H19, Scr-RNA (a nonspecific scrambled siRNA used as negative control), and their respective AAV-carried constructs were synthesized by Vigene Biosciences (Jinan, Shandong, China). The sequence were as follows: Sh-H19, sense: 5'-GCAGGUGA GUCUCCUUCUUTT-3'; and Scr-RNA, sense: 5'-UUCUCCGAACGUGUC ACGUdTdT-3'). The synthesis of an overexpression plasmid for H19, pEnter-H19 (GenBank Accession Number: NR_130973.1), and construction of the green fluorescent protein (GFP)-containing constructs AAV-GFP-H19 and AAV-GFP were performed by Vigene Biosciences (Jinan, Shandong, China). For the in vivo experiments, ApoE$^{-/-}$ mice were intraperitoneally injected with the AAV vector with Sh-H19 or Scr-RNA, and C57BL/6 J mice were injected with AAV-GFP-H19 or AAV-GFP (1 × 10^{11} vector genomes). For in vivo experiments evaluating the ceRNA mechanism of H19/let-7a/IL-6, C57BL/6 J mice were injected with AAV-GFP-H19 or AAV-H19-mut (H19 with an effectively mutated binding site to let-7a, H19-MUT1, see *Luciferase Report Assay* in

Materials and Methods, 1 × 10^{11} vector genomes). At 30 days after transfection, the ApoE$^{-/-}$ mice were randomly grouped and treated with Ang II or normal saline, as previously described. The C57BL/6 J mice were randomly treated with Ang II or normal saline or treated with CaCl$_2$ or normal saline, as previously described. For ex vivo studies, mouse aortic VSMCs and macrophages were separately seeded at 30–40% confluence in 6-well plates. After 24 h of culture, 50 nM siRNA or 4 μg of pEnter-H19 was randomly added to 250 μL of Opti-MEM medium (Gibco BRL, Paisley, UK) before the addition of 5 μL of Lipofectamine 3000 (Invitrogen, CA, USA). The mixed solution was incubated at room temperature for 0.5 h and then added to the cells. After 6 h of incubation, the medium was replaced with the same volume of DMEM at 37 °C. After 48 h, the cells were subjected to RNA or protein isolation. For ex vivo rescue experiments, briefly, mouse VSMCs or macrophages were cultured in DMEM for 24 h. Cells that were 30–40% confluent were incubated with si-H19 or a combination of si-H19 and mmu-let-7a inhibitor (miR20000521, Ribo Biotech, Guangzhou, China) or incubated with pEnter-H19 plasmids (pcDNA3.1-H19) or with a combination of pEnter-H19 plasmids and mmu-let-7a mimics (miR10000521, Ribo Biotech, Guangzhou, China). Twenty-four hours after incubation, the cells were stimulated with Ang II (10^{-7} mol/L, Sigma) for 24 h. Then, the cells were examined.

2.11. IL-6 rescue experiment

For the IL-6 rescue experiment, tocilizumab (TCZ, A2012, Selleckchem, Houston, USA), a monoclonal antibody against the IL-6 receptor, was used to suppress IL-6 signaling. Thirty days after transfection with AAV-H19, male C57BL/6 J mice were randomly treated with 2 mg of tocilizumab or an equal amount of IgG by tail vein injection. Twenty-four hours after treatment, all mice were perfused with Ang II for an additional 28 days, during which 0.25 mg of tocilizumab was intraperitoneally injected once a week to ensure the suppression of IL-6-mediated effects. Twenty-eight days after Ang II perfusion, the mice were sacrificed for examination.

2.12. Immunohistochemical analysis

The aortic samples were deparaffinized, and endogenous peroxidase activity was blocked by 3% (vol/vol) hydrogen peroxide, with subsequent preincubation with 10% bovine serum to block nonspecific binding sites [21]. The slides were next incubated at 4 °C overnight with primary antibodies and for 30 min with a biotinylated secondary antibody, followed by incubation in a horseradish peroxidase-labeled streptavidin solution. Then, the slides were stained with diaminobenzidine and counterstained with hematoxylin. The primary antibodies used were rabbit anti-α-SMA (ab32575, Abcam) for human AAA, and rabbit anti-IL-6 (ab7737, Abcam), rabbit anti-MCP1 (ab25124, Abcam), and rat anti-MAC-2 (CL89472AP, Cedarlane Laboratories, Ltd.) for both Ang II- and CaCl$_2$-induced aortic aneurysms. Negative control experiments were performed to confirm the specificity of antibody binding in Ang II-treated ApoE$^{-/-}$ mice.

2.13. Western blotting (WB)

Protein levels of MCP-1 and β-actin in mouse aortas, cultured
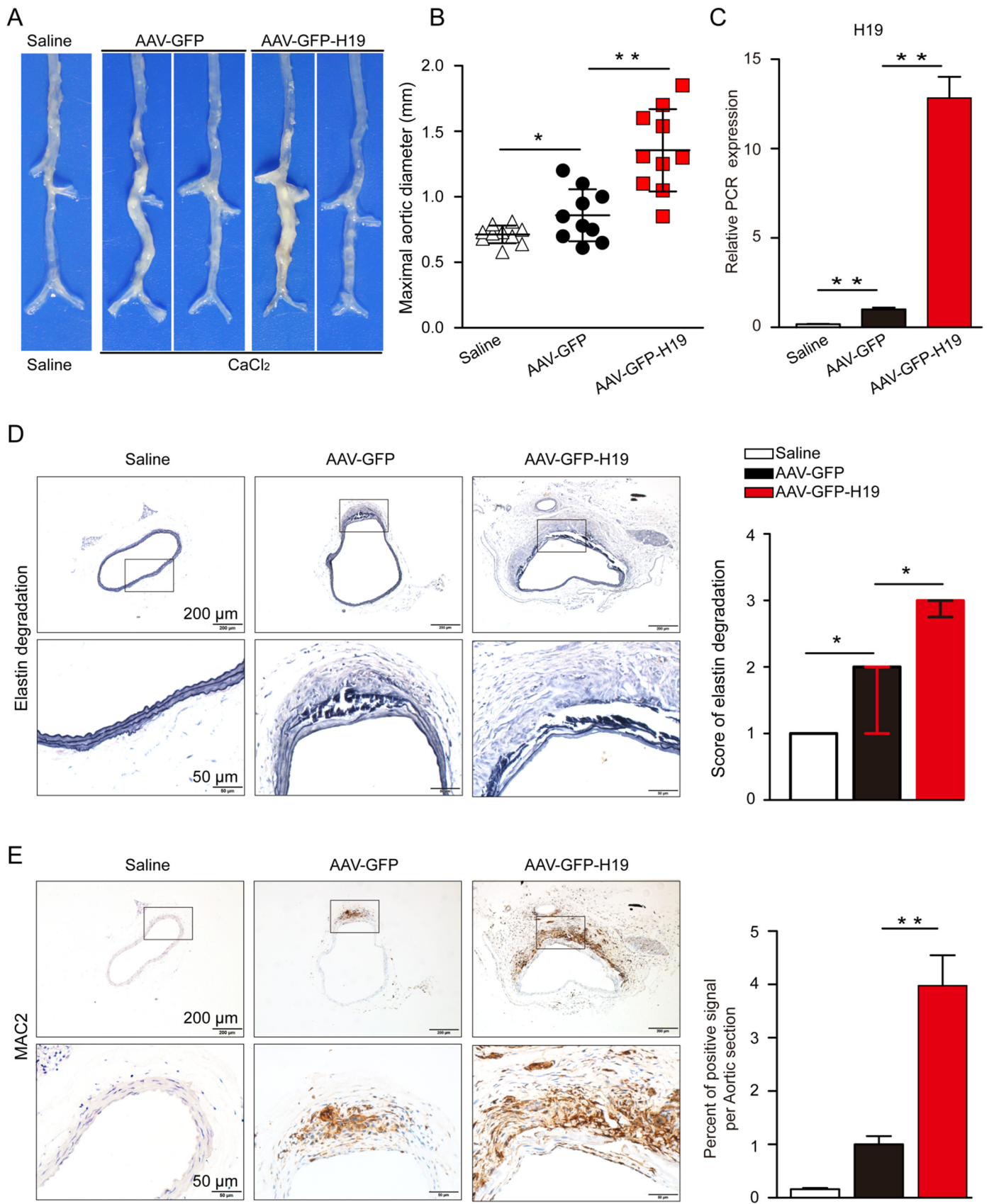
(caption on next page)

Fig. 4. H19 overexpression promotes AAA formation in CaCl$_2$-treated C57BL/6J mice.
Male C57BL/6J mice were injected with the viral vector AAV-GFP-H19 or AAV-GFP 30 days before treatment of the suprarenal aorta with CaCl$_2$ gauze ($n = 25$ in each group). Saline, male C57BL/6J mice with sham normal saline injection were treated with an equal amount of normal saline ($n = 10$). Detection was carried out 3 weeks after CaCl$_2$ treatment. (A) Representative photographs of AAA. (B) Maximal aortic diameter of the abdominal aorta ($n = 10$ per group). (C) Statistical analysis of RNA levels of aortic H19 after virus injection ($n = 4$ per group). (D) Representative elastin staining and elastin degradation scores in mouse aortas. Photographs show the location where the most severe elastin degradation occurred (n = 10 per group; scale bars: upper 200 μm, lower 50 μm; magnified photographs). (E) Representative immunofluorescence staining and statistical analysis of aortic MAC-2 protein expression (n = 4 per group, scale bars: upper 200 μm, lower 50 μm; magnified photographs). The data are presented as the mean ± SD or as the median and IQR (for elastin degradation score). **$P < .01$.

VSMCs, and cultured macrophages were measured using the WB technique, as previously described [22]. Identical amounts of protein from mouse aortic tissues or cells containing identical amounts of protein were denatured and resolved via 12% SDS-PAGE using a 10% running gel. Proteins were dissociated using 10% SDS-PAGE and probed with primary antibodies for MCP1 (ab25124, Abcam) or β-actin (ab5694, Abcam) at 4 °C overnight, and the membranes were washed and incubated with an HRP-conjugated anti-rabbit secondary antibody at a 1:5000 dilution (DAKO) for 2 h. β-actin was used as a loading control.

Bands were detected using enhanced chemiluminescence (ECL Advance™; #RPN2235, GE Healthcare Life Sciences) on a GeneGnome XRQ chemiluminescence imaging system (Syngene, MD, U. S. A.). ImageJ software was used to calculate the relative density of proteins. All experiments were repeated 3 times.

2.14. Quantitative real-time PCR

Total RNA from cultured VSMCs, macrophages, or mouse aortic tissues was extracted by homogenization using TRIzol (Invitrogen) according to the manufacturer's instructions. cDNA was synthesized by using reverse transcriptase (Invitrogen) with the following primers, which were synthesized by Saicheng Biotech (Guangzhou, China): H19, 5′-AAGCAGATGGAACAGGTGGC-3′ (forward), 5′-CACAGCCAAACTGC CCAAAG-3′ (reverse); RNCR3, 5′-GCTTCTTAGTGCTCTGTCTA-3′ (forward), 5′-GATGGATGGATGGATGGATT-3′ (reverse); Tug1, 5′-AGAGA CACGACTCACCAAGC-3′ (forward), 5′-GGCAGGTCCAGGTGAACATT-3′ (reverse); MEG3, 5′-AGCGGGAGTGTTAAGCTAGGC-3′ (forward), 5′-ATTGAGTCACCTGCAAGCGT-3′ (reverse); Hotair, 5′-CCAGCGCTAA GTCCTTCCAG-3′ (forward), 5′-TTTCTCCGTGCGTGTCTTCT-3′ (reverse); Miat, 5′-ATGCCTCACCTCCAGTAG-3′ (forward), 5′-TGCTCAGT AGACAGTATCCT-3′ (reverse); IL-6, 5′-CCGCTATGAAGTTCCTCTC-3′ (forward), 5′-GGTATCCTCTGTGAAGTCTC-3′ (reverse); MCP1, 5′-ACC TGCTGCTACTCATTCAC-3′ (forward), 5′- CATTCAAAGGTGCTGAA GAC-3′ (reverse); β-actin, 5′-GGCTGTATTCCCCTCCATCG-3′ (forward), 5′- CCAGTTGGTAACAATGCCATGT-3′ (reverse); let-7a, 5′-CGCTTGGT GAGGTAGTAGGTTGT-3′ (forward), 5′-ATCCAGTGCAGGGTCCGAGG-3′ (reverse); miR-21, 5′-GCGCGTAGCTTATCAGACTGA-3′ (forward), 5′-AGTGCAGGGTCCGAGGTATT-3′ (reverse); and U6, 5′-CTCGCTTCG GCAGCACA-3′ (forward), 5′-AACGCTTCACGAATTTGCGT-3′ (reverse). Quantitative real-time PCR (qRT-PCR) was performed with a SYBR Green RT-PCR Kit (Invitrogen) using the Luminaris Color HiGreen High ROX qPCR Master Mix (Thermo Fisher Scientific, Waltham, MA) with a Light Cycler 480 II (Roche Diagnostics, Basel, Switzerland). Relative RNA expression of the gene or the lncRNA was determined using the 2-ΔΔCt method by normalizing to β-actin expression. For the quantification of microRNA expression, U6 was used as an endogenous normalizer.

2.15. Immunofluorescence staining

For the suprarenal aorta, frozen sections were incubated with rabbit anti-GFP (1:50, Santa Cruz Biotechnology) or rat anti-MAC-2 (CL89472AP, Cedarlane Laboratories, Ltd.), and then with a secondary fluorescein isothiocyanate (FITC)-conjugated goat anti-rabbit IgG/FITC antibody (Bioss bs-0295G-FITC) (1:100) (Zhongshan Golden Bridge Biotechnology, Beijing) or donkey anti-rat IgG (ab150154, Alexa Fluor

555), respectively. DAPI (BB-4133-100T, BestBio Science) was used for cellular nuclei immunofluorescence staining. For ex vivo VSMCs, the cells were prepared as described and then fixed with paraformaldehyde (4%), washed with PBS, incubated with a goat serum blocking solution (10%), incubated with rabbit anti-IL-6 antibodies (1:100) and mouse anti-α-SMA antibodies (1:100), washed 3 times with PBS and incubated in fluorescein-conjugated secondary antibodies (goat anti-rabbit IgG/ Alexa Fluor 555 antibody (Bioss bs-0295G-AF555), red; goat anti-mouse IgG/FITC antibody (Bioss bs-0296G-FITC), green; 1:100). Then, the VSMCs were washed with PBS and mounted with 4′,6-diamidino-2-phenylindole (DAPI). For negative controls, the primary antibody was replaced by IgG. The fluorescence signal was visualized by a fluorescence inverted/laser scanning confocal microscope (Leica Imaging Systems, Cambridge, UK).

2.16. IL-6 ELISA

IL-6 concentrations in mouse plasma as well as in ex vivo culture solution were measured using a mouse IL-6 ELISA kit (CSB-E04639m, Cusabio Biotech) according to the manufacturer's instructions.

2.17. LncRNA in situ hybridization

In situ hybridization was implemented to detect H19 content and distribution in the mouse aorta. Aortic specimens were embedded in paraffin and cut into sections 4 mm thick and 2 mm in diameter to construct microarrays. After digestion by proteinase K, the microarray was hybridized to a digoxin-tagged and LNA™-modified H19 probe (TCTCCATCACACCGGACCATGT/3Dig_N/− custom LNA mRNA detection probe, 250 nmol, RNA Tm: 85 °C, DNA Tm: 78 °C, Yield: 0.5 OD/ 2.6 nmol/21.4 μg) via incubation at 55 °C overnight. Then, the samples were incubated overnight with an anti-digoxin-AP Fab fragment. The cytoplasm was stained with NBT/BCIP in the dark, and the in situ hybridization signal of H19-AS1 was identified as a blue-purple speckle. Afterwards, some of the samples were subjected to immunofluorescence staining (co-staining) as described above.

2.18. Luciferase reporter assay

Luciferase reporter assay procedures were performed as previously described [23]. A luciferase reporter assay was performed to confirm the binding sites between IL-6 and let-7a and between let-7a and H19 in cultured VSMCs and macrophages. We embedded the 3′ untranslated region (UTR) of IL-6 into the pMIR-GLO dual-luciferase carrier to induce mutations in the region and constructed a number of nucleotide mutations within the IL-6 3' UTR. The generated plasmids were transiently transfected into the cells pretreated with functional let-7a analogs or into cells in the corresponding control groups. The cells were incubated for 48 h, then acquired and dissolved. Luciferase activity within the cells was detected according to the dual-luciferase reporter system illustration (Promega, United States) and was regarded as an indicator of an intracellular interaction between let-7a and IL-6. Similarly, the pMIR-H19–3' UTR was used to construct a mutant H19 3' UTR, which was then transfected into cells with similar functional let-7a analogs or into control groups. The cells were incubated, and intracellular luciferase activity was detected.
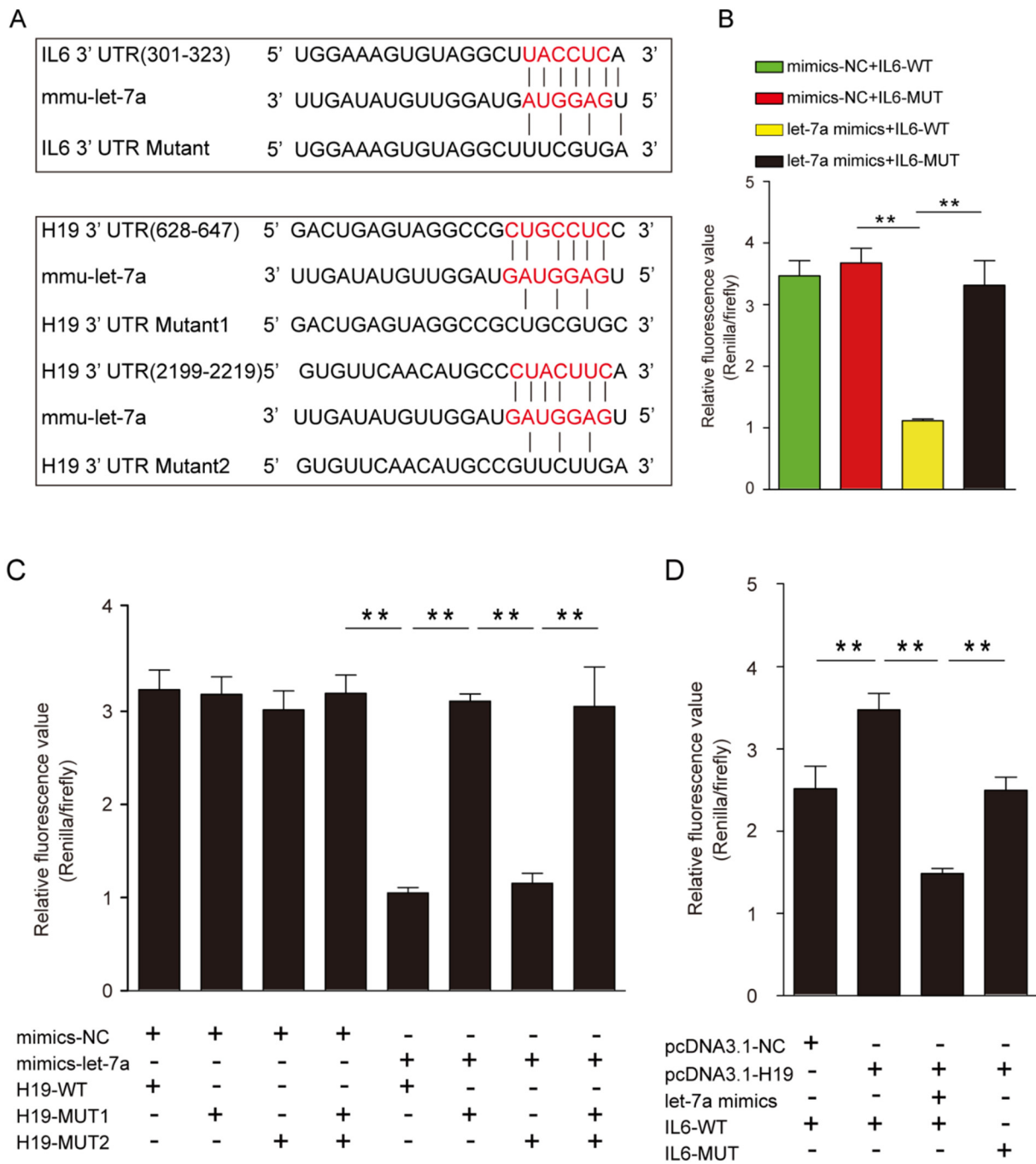
Fig. 5. H19 functions as a let-7a sponge in VSMCs.
(A) Potential binding sites between H19 and let-7a and between IL-6 and let-7a and the constructed mutant binding sites. (B) Results of the luciferase reporter gene assay. VSMCs were transiently transfected with a functional let-7a mimics or an invalid let-7a analog (mimic-NC). Twenty-four hours later, the cells were transfected with a luciferase reporter containing wild-type IL-6 (IL-6-WT) or mutant IL-6 (IL-6-MUT). Luciferase activity was analyzed after 24 h. (C) Results of the dual-luciferase reporter gene assay. VSMCs were transiently transfected with a functional let-7a analog (let-7a mimics) or an invalid let-7a analog (mimic-NC) and then transfected with a luciferase reporter containing wild-type (H19-WT) or mutant H19 (H19-MUT1, H19-MUT2). Luciferase activity was analyzed after 24 h. (D) Results of a dual-luciferase reporter gene assay. The cells were transiently transfected with functional plasmid-mediated H19 transcripts (pcDNA3.1-H19) or sham transcripts (pcDNA3.1-NC), and functional let-7a mimics was selectively added. Then, the cells were transfected with a luciferase reporter containing wild-type IL-6 (IL-6-WT) or mutant IL-6 (IL-6-MUT). Luciferase activity was analyzed after 24 h. $^{**}P < .01$. Experiments were performed in quadruplicate.

2.19. Statistical analyses

The values are presented as the mean ± SD or as the median and interquartile range (IQR, for elastin degradation score). The data were analyzed using SPSS version 20.0 (SPSS, Inc., Chicago, IL, USA). Normality tests were assessed via Shapiro-Wilk statistics. Student's *t*-tests were used for normally distributed datasets when statistically comparing the data from two groups. Differences among groups were determined using one-way ANOVA, followed by the least significant difference (LSD) post hoc test or Dunnett test. Fisher's exact test was used to analyze of aneurysm morbidity. When a normal distribution could not be determined, nonparametric tests were used (Mann-Whitney *U* test for 2 independent groups, Wilcoxon signed rank test for 2 paired groups and the Kruskal-Wallis test with post hoc Dunn's
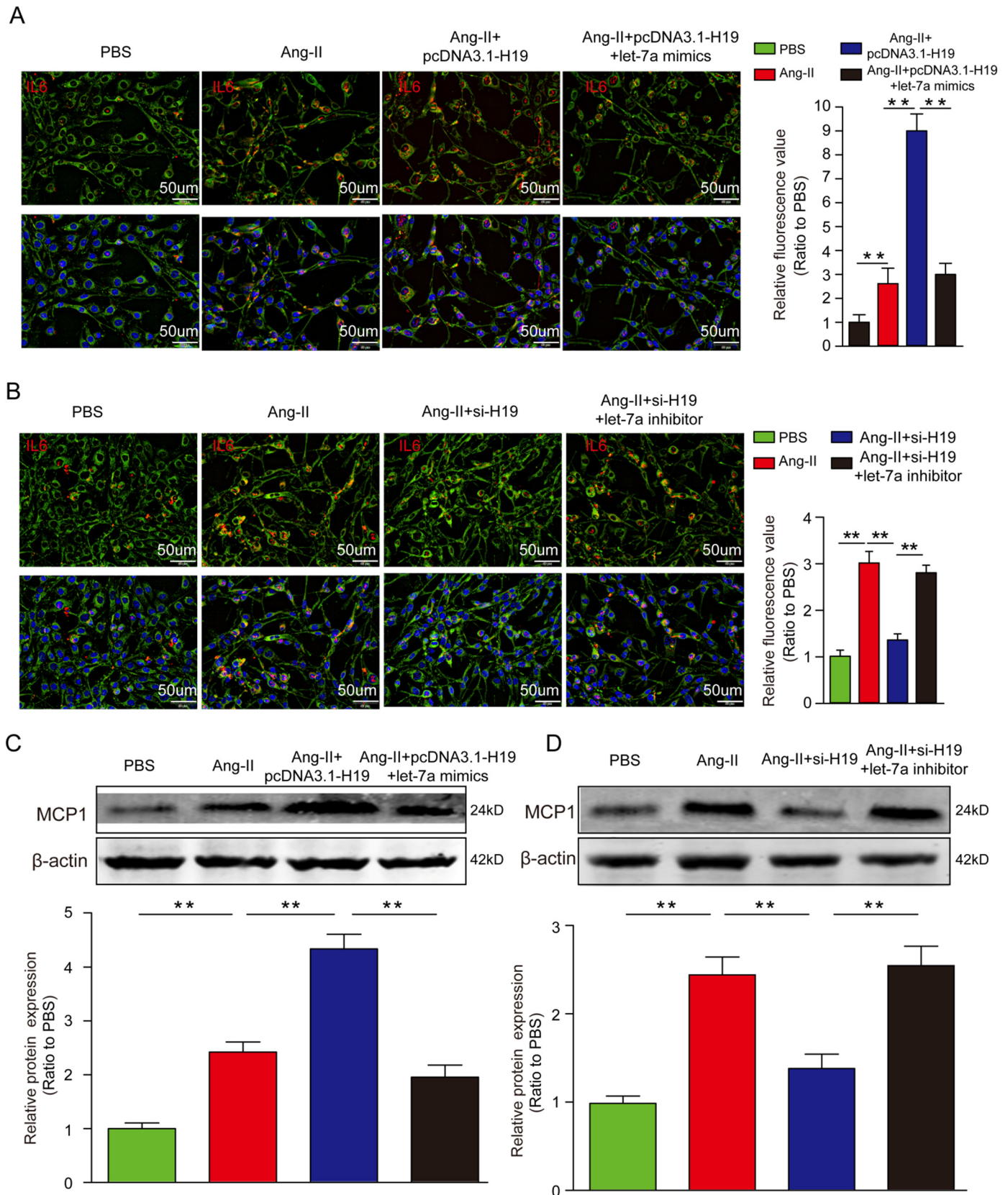
Fig. 6. Aortic H19 targets and negatively regulates let-7a to promote IL-6 expression in VSMCs.
Mouse aortic VSMCs were cultured for 24 h. Then, the cells were incubated with pcDNA3.1-H19 plasmids or a combination of pcDNA3.1-H19 plasmids and let-7a mimics, or the cells were incubated with si-H19 or a combination of si-H19 and a let-7a inhibitor. Twenty-four hours later, the cells were stimulated with Ang II (10^{-7} mol/L) for another 24 h. (A and B) Dual-luciferase reporter gene assay results. Alterations to IL-6 expression after H19 transfection and/or functional let-7a mimic administration (A), or after aortic H19 knockdown and/or let-7a inhibition (B). (C and D) WB analysis of MCP-1 expression within VSMCs after H19 transfection and/or functional let-7a mimic administration (C), or after aortic H19 knockdown and/or let-7a inhibition (D). $^{**}P < .01$. Experiments were performed in quadruplicate.
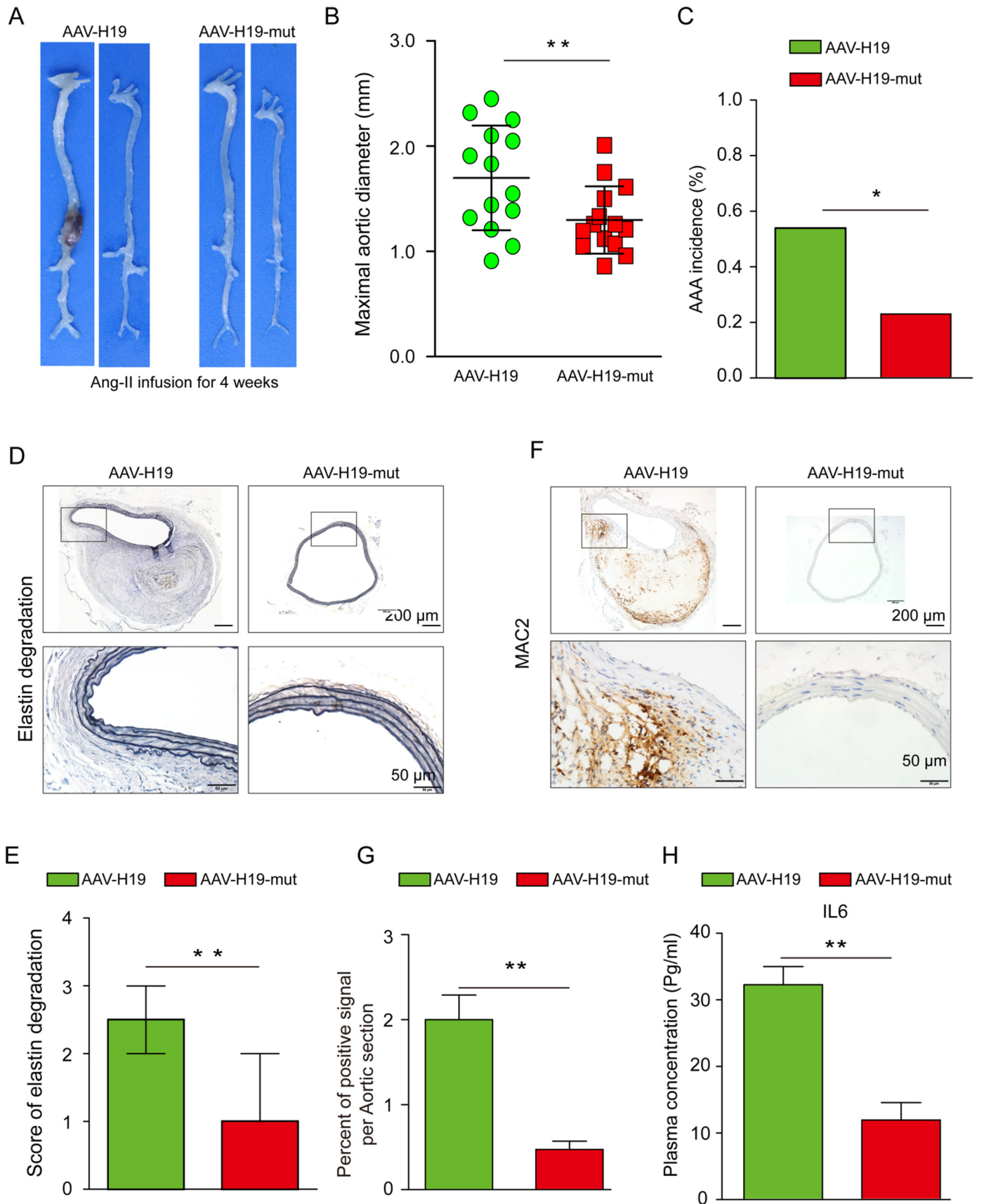
(caption on next page)

Fig. 7. Higher let-7a bioactivity alleviates AAA formation in Ang II-treated C57BL/6 J mice.
Male C57BL/6 J mice were transfected with AAV-H19 or AAV-H19-mut (*n* = 26 per group). Thirty days later, they were infused with Ang II for an additional 28 days. (A) Representative images of macroscopic features of the aorta. (B) Maximal aortic diameter of the abdominal region (*n* = 14 per group). (C) Statistical analysis of AAA incidence (n = 26 per group). (D and E) Representative elastin staining (D) and elastin degradation scores (E) in aortas. Images show the location where the most severe elastin degradation occurred (n = 14 per group; scale bars: upper 200 μm, lower 50 μm; magnified images). (F and G) Representative immunofluorescence staining of aortic MAC-2 (F) and its statistical analysis (G) (*n* = 4 per group; scale bars: upper 200 μm, lower 50 μm; magnifiedimages). (H) Plasma IL-6 concentration (*n* = 8 per group). The data are presented as the mean ± SD or as the median and IQR (for elastin degradation score). *P < .05, **P < .01.

multiple comparisons test for ≥ 3 groups). We calculated the significance of each treatment as a *P* value, and *P* < .05 was considered statistically significant (The statistical approaches used in the study are shown in Supplemental Table S2).

3. Results

3.1. LncRNA H19 is re-expressed in human AAA and Ang II- and CaCl₂-induced mouse AAA

Based on emerging evidence that certain lncRNAs possess crucial regulatory functions in some vascular inflammatory disorders, we first searched for published lncRNAs that are associated with inflammation. By reading full-text literature in PubMed after searching the results one by one, twenty-six known lncRNAs were included (Table S1). Next, these twenty-six lncRNAs were individually retrieved one by one in PubMed to determine whether they were associated with vascular histology. The full text of each publication in the literature was carefully read, and ten vascular inflammation-associated lncRNAs were obtained (Table S1). Among them, six lncRNAs (H19, TUG1, MEG3, HOTAIR, MIAT, RNCR3) were homologous between human and mouse. We then performed qRT-PCR to examine the expression levels of these six lncRNAs in Ang II-perfused ApoE⁻/⁻ mouse AAA. Of these six lncRNAs, H19 was most strikingly upregulated in AAA (Fig. S1B) and was chosen for further investigation.

To determine whether H19 was re-expressed during AAA pathogenesis, we detected H19 expression in human and mouse AAA. Human AAA sections and adjacent normal specimens were obtained from patients undergoing AAA surgery. Human AAA formation was confirmed by substantially reduced levels of alpha-smooth muscle actin (α-SMA), a robust marker of smooth muscle cells (SMCs) (Fig. S1C). The qRT-PCR results showed that the expression of H19, as well as the RNA levels of IL-6 and MCP-1, two crucial proinflammatory molecules typically implicated in AAA formation, were significantly increased in human AAA sections (Fig. 1A–C). We next investigated the expression of H19 in mouse AAA. As previously described, male ApoE⁻/⁻ mice were infused with Ang II or an equal amount of normal saline using a minipump for 4 weeks, and male C57BL/6 J mice were treated with CaCl₂ gauze or an equal amount of normal saline gauze for 15 min during surgery. As evident by macroscopy, obvious bulges were observed in Ang II-infused and CaCl₂-treated mice but not in their control counterparts (Fig. S1A). The levels of H19 detected by qRT-PCR and in situ hybridization were substantially increased in aortas from both AAA models relative to those from control mice (Fig. 1D–G). To determine the localization of H19 in AAA, we performed co-staining that combined in situ hybridization of H19 and immunofluorescent staining of macrophages (MAC-2) in aortic samples from both Ang II-perfused and CaCl₂-treated mice (Fig. 1E and G). We found that H19 was located not onlyin VSMCs but also in abundantly infiltrating macrophages, as evidenced by the overlap between signals of H19 and MAC-2 in both murine AAA models. To further explore the cellular location of H19, immunohistochemical staining with α-SMA and in situ hybridization of H19 were performed in ex vivo VSMCs. High-magnification microscopic images of the immunofluorescence staining of α-SMA and the in situ hybridization of H19 showed that H19 was mainly located in the cytoplasm (Fig. S1D and E). Taken together, our data revealed the upregulation of H19 expression in both human and animal AAA.

3.2. Reduction in the level of H19 suppresses Ang II-induced AAA formation in ApoE⁻/⁻ mice, and H19 overexpression exacerbates AAA development in Ang II-induced C57BL/6 J mice

To further determine whether there is a causative link between disrupted H19 expression and AAA development, we applied AAVs carrying H19-interfering (Sh-H19 group) or overexpression constructs (AAV-GFP-H19 group) and corresponding sham control viruses (Scr-RNA group and AAV-GFP group) to perform gain- and loss-of-function studies in Ang II-perfused mice. For a fair assessment, mice without AAA induction (Saline, sham perfusion with normal saline) were included. First, to first determine viral intervention potency, Sh-H19 or Scr-RNA and AAV-GFP-H19 or AAV-GFP were separately transfected into ApoE⁻/⁻ and C57BL/6 J mice (without later Ang II intervention), respectively. GFP signals were detected to reflect viral intervention potency. Compared with the saline group, the four transfected groups had significantly enhanced aortic GFP signals at 30 days after transfection, indicating abundant virus expression (Fig. S2A and B). Indeed, from the 15th day onward, both the knockdown and overexpression interventions exhibited the anticipated H19 expression, and these trends remained stable and significant through the 60th day (Fig. S2C and D).

Based on the efficient and stable H19 control, Ang II infusion was performed starting on the 30th day and lasted for 28 days in both ApoE⁻/⁻ and C57BL/6 J mice, and CaCl₂ treatment was also performed on this day in other C57BL/6 J mice. Aortic H19 expression was significantly downregulated in the Sh-H19 group of ApoE⁻/⁻ mice on the 28th day after Ang II treatment (Fig. S3A). AAA formation was alleviated in Sh-H19 mice relative to their sham counterparts, which had a substantial bulge in the abdominal aorta, as seen by macroscopy (Fig. 2A). Ultrasound imaging also confirmed this change (Fig. 2B). Aortic aneurysm incidence and the maximal aortic diameter were substantially decreased in the Sh-H19 group (Fig. 2C and D). Ang II-induced elastin degradation, as indicated by immunohistochemical staining and elastin degradation scores, was effectively prevented in Sh-H19 mice, in contrast to Scr-H19 mice (Fig. 2E). As proinflammatory molecules IL-6 and macrophage infiltration induce AAA initiation and progression, we examined the effect of H19 intervention on the expression levels of IL-6 and MAC-2 (a macrophage marker) after 28 days of Ang II infusion. Aortic MAC-2 protein and mRNA expression were significantly decreased in the ApoE⁻/⁻ mice in the Sh-H19 group (Figs. 2F and S3A), as were aortic protein mRNA and protein levels of IL-6 (Fig. S3A and B), plasma IL-6 (Fig. S3C), and aortic MCP-1 (Fig. S3A and D), indicating alleviated proinflammatory responses upon H19 deficiency. In addition, H19 deficiency had no significant effect on the systolic BP of the mice (Fig. S3E), suggesting that this protective effect against AAA was not dependent on BP alleviation.

Next, a gain-of-function experiment was carried out in C57BL/6 J mice. In the AAV-GFP group and the AAV-GFP-H19 group, on the 28th day after Ang II treatment, aortic H19 expression was significantly upregulated, as anticipated (Fig. S4A). C57BL/6 J mice subjected to H19 overexpression had a substantial bulge in the abdominal aorta, as seen by macroscopy and ultrasound imaging (Fig. 3A and B). Aortic aneurysm morbidity and the maximal aortic diameter were substantially higher in the AAV-GFP-H19 group (Fig. 3C and D). Consistent with these findings, elastin degradation of the aorta was significantly exacerbated (Fig. 3E), and aortic protein levels of MAC-2 were
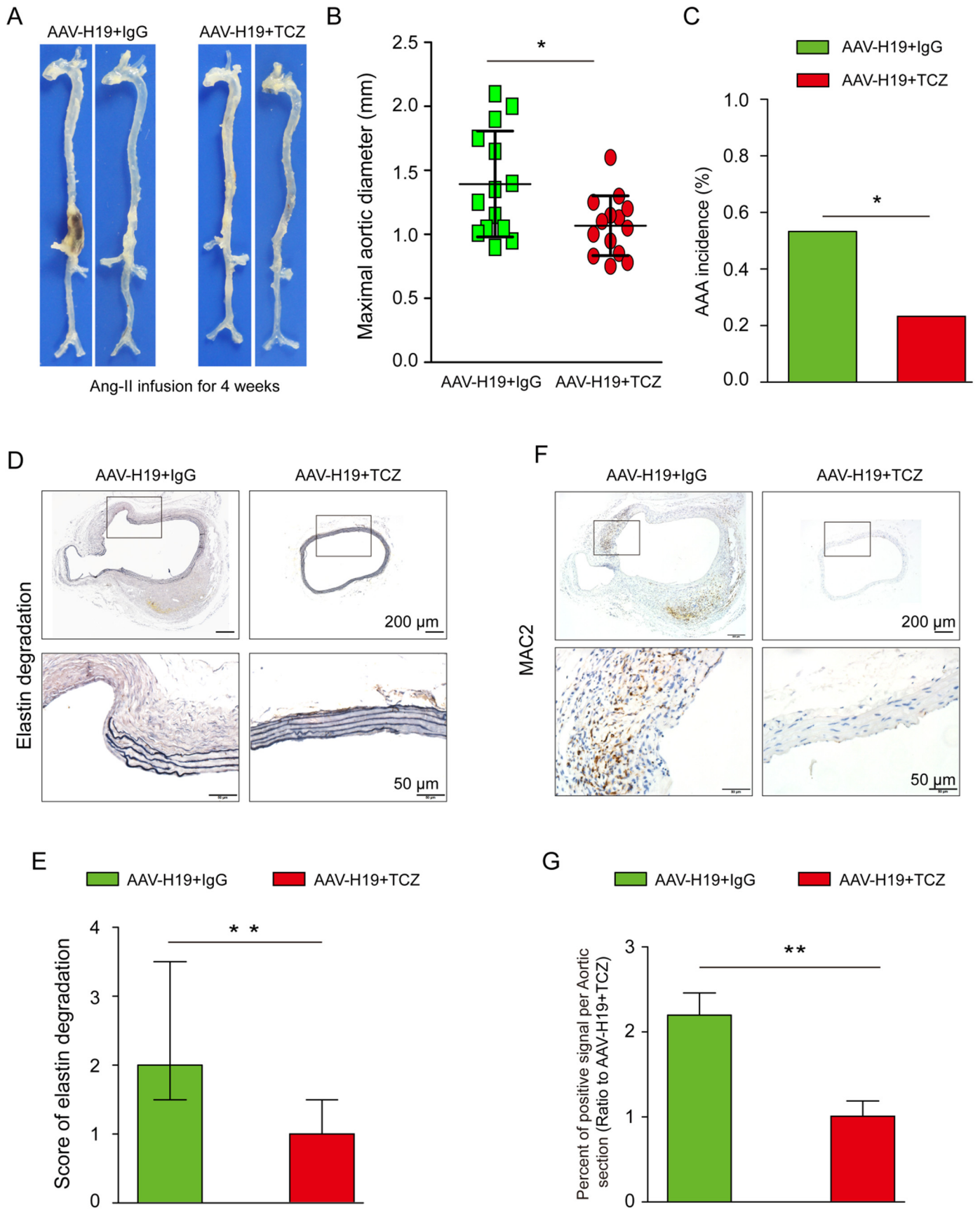
(caption on next page)

Fig. 8. Confirmation of the inflammation intermediary role of IL-6 during H19-promoted AAA formation.
Male C57BL/6 J mice were transfected with AAV-H19. Thirty days later, they were randomly treated with tocilizumab (TCZ, a monoclonal antibody against IL-6 receptor) or an equal amount of IgG ($n = 30$ per group). Twenty-four hours after treatment, all mice were perfused with Ang II for an additional 28 days and then sacrificed for examination. (A) Representative images of macroscopic aortas in the two groups. (B) Maximal aortic diameter of the abdominal region ($n = 14$ per group). (C) Statistical analysis of AAA incidence (n = 30 per group). (D and E) Representative elastin staining (D) and elastin degradation scores (E) in aortas. Images show the location where the most severe elastin degradation occurred (n = 14 per group; scale bars: upper 200 μm, lower 50 μm; magnified images). (F and G) Representative immunofluorescence staining of aortic MAC-2 (F) and its statistical analysis (G) ($n = 5$ per group; scale bars: upper 200 μm, lower 50 μm; magnified images). The data are presented as the mean $\pm$ SD. *$P < .05$, **$P < .01$.

substantially elevated in the AAV-GFP-H19 group (Fig. 3F), as were aortic IL-6 and MCP-1 mRNA levels, the plasma IL-6 concentration (Fig. S4A and B), and aortic MCP-1 protein levels (Fig. S4A and C). Thus, our findings confirmed that H19 upregulation causes AAA induction, which is associated with enhanced vascular inflammation and that H19 deficiency exerts a protective effect against AAA formation.

3.3. Disruption of H19 promotes AAA formation in CaCl₂-induced C57BL/6 J mice

To explore whether the effects of aortic H19 disruption on AAA formation are partly associated with the CaCl₂ pathway, we introduced the well-accepted CaCl₂-induced AAA model in the context of H19 overexpression. For a fair assessment, mice without AAA induction (Saline, sham treatment with normal saline) were included. Three weeks after the initial CaCl₂ application, obvious AAA formation was seen, and the maximal aortic diameter of the aneurysm was significantly elevated in the AAV-GFP-H19 group relative to that in the AAV-GFP group (Fig. 4A and B). As expected, murine aortic H19 was successfully upregulated in the AAV-GFP-H19 group (Fig. 4C). In addition, elastin fragmentation was more severe in the AAV-GFP-H19 group (Fig. 4D). Protein levels of aortic MAC-2 were also markedly enhanced (Fig. 4E), as were mRNA, plasma, and protein levels of IL-6 (Fig. S5A to C) and MCP-1 (Fig. S5A and D) in the aortas of the AAV-GFP-H19 group relative to those of the AAV-GFP group. These results indicate that H19 exacerbates AAA formation and related inflammatory pathological changes in a CaCl₂-related manner.

3.4. H19 functions as a let-7a sponge in VSMCs and macrophages

Given that H19 is a lncRNA that is abundant in the cytoplasm and that lncRNAs of this kind often function through a ceRNA mechanism, we next explored whether H19 regulates AAA development in this manner. Bioinformatics predictions using StarBase indicated that the H19 sequence contained two let-7a binding sites. Next, we used the online tool TargetScan and focused on key inflammatory molecules during AAA development. Among the putative targets of let-7a, we focused on the gene encoding IL-6. To determine the direct interactions between let-7a and the IL-6 3' UTR and between let-7a and the H19 3' UTR, we mutated the let-7a binding site in IL-6 to generate Luc-IL-6-mut, and we mutated the let-7a binding site in H19 to generate Luc-H19-mut (Fig. 5A). Functional (let-7a mimics) and invalid (mimics-NC) let-7a analogs and functional (pcDNA3.1-H19) and invalid (pcDNA3.1-NC) plasmid-mediated H19 overexpression constructs were also constructed. Luciferase reporter gene assay results showed that let-7a directly targets IL-6 (Fig. 5B). Mutant H19 reversed the luciferase activity results relative to those of wild-type (WT) H19 (Fig. 5C) when there was a sufficient level of functional let-7a mimics, proving that let-7a directly targets H19. Furthermore, in Luc-IL-6-WT, transfection with pcDNA3.1-H19 upregulated luciferase activity, which was inhibited by let-7a mimics. As expected, the in Luc-IL-6-mut, transfection with pcDNA3.1-H19 had no impact on luciferase activity (Fig. 5D). Experiments on Ang II-treated macrophages obtained similar results to those in VSMCs (Fig. S7). On the other side, we examined the let-7a expression in vivo. qRT-PCR results showed no significant difference in let-7a levels in Ang II-induced AAA in C57BL/6 J mice relative to normal saline-perfused

mice, suggesting that let-7a bioavailability, rather let-7a levels, was altered under Ang II induction. The comparable content between let-7a and miR-21 (an abundantly expressed microRNA under Ang II stimulation) confirmed the high let-7a expression in mice (Fig. S6B).

3.5. H19 induces AAA formation by promoting expression of the let-7a target IL-6 in VSMCs and macrophages and in Ang II-treated C57BL/6J mice

Next, we evaluated whether H19 regulates IL-6, the downstream target of let-7a in VSMCs and macrophages. Ang II treatment remarkably enhanced cellular H19 expression in macrophages (Fig. S7A). An ex vivo dual-luciferase reporter gene assay in VSMCs showed that IL-6 expression induced by H19 overexpression was substantially reversed by additional let-7a mimics (Fig. 6A), while IL-6 suppression caused by H19 downregulation was prevented when a let-7a inhibitor (monoclonal antibody) was added (Fig. 6B). WB results for MCP-1 protein expression also corresponded to our IL-6 expression results (Fig. 6C and D). In addition, in Ang II-treated macrophages, intracellular IL-6 mRNA levels, IL-6 concentration in culture solution and intracellular MCP-1 protein levels showed similar trends to those found in Ang II-treated VSMCs (Fig. S8A–D). Thus, our results indicated that IL-6 is a direct target of let-7a and that H19 regulates IL-6 expression by endogenously competing with let-7a, confirming the H19/let-7a/IL-6 pathway in both cells.

To further validate the conclusion obtained from ex vivo experiments, we introduced in vivo experiments overexpressing either wild-type H19 (AAV-H19) or mutant H19 (H19-MUT1) that is unable to bind let-7a (AAV-H19-mut) in C57BL/6 J mice (Fig. 7), causing higher bioactive let-7a levels in the latter group. After 28 days of Ang II perfusion, mice in AAV-H19-mut group showed substantially reduced AAA formation, decreased maximal aortic diameter, lower plasma IL-6 levels, and alleviated elastin degradation and macrophage infiltration when compared with the AAV-H19 group (Fig. 7A–H). These in vivo data robustly support that H19 acts as a competing endogenous let-7a sponge to increase IL-6 expression during AAA development.

3.6. H19 transmits vascular inflammation and promotes AAA formation through intermediary IL-6

To prove a causal relationship between AAA formation and IL-6 upregulation and explore whether the "H19/let-7a/IL-6 inflammatory pathway" is important for AAA pathogenesis, we designed an IL-6 rescue experiment. We found that IL-6R neutralization substantially reduced AAA formation, decreased the maximal aortic diameter, and mitigated the elastin degradation and macrophage infiltration that were evoked by H19 overexpression (Fig. 8A–G). These results provide in vivo causal evidence for a link between IL-6 and Ang II-induced AAA formation, supporting the proposal that H19 transmits vascular inflammation and promotes AAA formation by using IL-6 as an intermediary.

4. Discussion

Here, we provide in vivo and ex vivo evidence that lncRNA H19 is pathogenic during AAA formation. We showed that H19 was re-

expressed in Ang II-induced adult mouse aortic aneurysms. H19 over-expression promoted AAA formation by enhancing vascular proin-flammatory IL-6 and MCP-1 and enhancing macrophage infiltration, while H19 deficiency reduced AAA formation by alleviating the ex-pression of these molecules after Ang II infusion. Of note, blockage of the IL-6 receptor substantially mitigated the pro-aneurysmal and proinflammatory effects of H19 overexpression, demonstrating the crucial intermediary role of IL-6 in H19-promoted AAA formation. We further found that H19 mediated aneurysm formation through a ceRNA mechanism by relieving the inhibitory effect of let-7a on IL-6 tran-scription in both VSMCs and macrophages and, more importantly, in an Ang II-induced AAA model.

LncRNAs have emerged as critical regulators of cardiovascular dis-eases, including cardiac hypertrophy [24,25], cardiac regeneration [26,27] and atherosclerosis [28]. By searching for published lncRNAs that are related to vascular inflammation in combination with concerns about species homology, we first identified six lncRNAs. Among them, H19 was the most strikingly upregulated lncRNA in mouse AAA. Our further experiments confirmed that upregulated H19 induces AAA formation. Aortic overexpression of H19 increased AAA morbidity, which was supported by intensified aortic enlargement, elastin de-gradation, and macrophage recruitment, while H19 deficiency alle-viated AAA formation and related pathological changes. A recent study provided robust in vivo evidence that H19 initiates AAA; however, this effect involves the induction of VMSC apoptosis [14]. Our results showed that H19 promotes AAA by exacerbating aortic inflammation, which is supported by our finding that H19 overexpression upregulated aortic mRNA and protein levels of the proinflammatory molecules IL-6 and MCP-1 and increased macrophage infiltration, all of which are factors that are known to affect AAA development, progression, and even rupture [3,4,29–31]. H19 repression showed the opposite effects. Similar to H19 upregulation-induced SMC apoptosis, our finding that H19 upregulation initiates AAA through vascular inflammation implies preventative and therapeutic significance. Physiopathologically, SMC apoptosis occurs late during AAA, while inflammatory responses occur early and are sustained throughout AAA development and progression, even in part by mediating SMC apoptosis [32]. On the other hand, aneurysmal wall inflammation is the key inducer of proteinase activa-tion, such as matrix metalloproteinase (MMP), one of the major effec-tors that degrades the extracellular matrix and directly causes aneurysm formation [33,34]. Accordingly, H19-mediated aortic inflammation might also be a potent driver mediating AAA formation, at least during the early and middle stages of the disease. Thus, interventions targeting vascular inflammation might be more beneficial for AAA prevention and treatment.

The term ceRNA refers to the fact that lncRNAs impact target gene mRNA expression by acting as microRNA molecular sponges [35,36]. In our study, according to the bioinformatics analysis results, we predicted that H19 could affect IL-6 levels by endogenously competing with let-7a. To determine the role of the H19/let-7a/IL-6 pathway in AAA for-mation, we designed luciferase experiments and rescue experiments using cultured VSMCs and macrophages and successfully examined the interactions between let-7a and IL-6, H19 and let-7a, and H19/let-7a/IL-6. IL-6 expression was markedly inhibited when functional let-7a mimics were added to cultured VSMCs or when there was a valid mu-tation in the H19-let-7a base-pairing region. In addition, this inhibition was thwarted when there was a valid mutation in the binding site be-tween the let-7a and IL-6 pairing sequences or when functional H19 mimics were present. Further in vivo experiments using mutant H19 unable to bind let-7a substantially mitigated AAA formation, elastin degradation and macrophage infiltration in Ang II-induced AAA mice. Therefore, we concluded that H19 acts as an endogenous let-7a sponge to increase the expression of IL-6 during AAA development. This ceRNA mechanism that underlies the H19/let-7a/IL-6 pathway is supported by a cholangiocarcinoma model, in which H19 is upregulated by oxidative stress and in turn enhances IL-6 expression and tumor cell migration

through let-7a inhibition [12]. Thus, our findings highlight the poten-tial of H19 inhibition to prevent or slow AAA progression by harnessing IL-6 expression.

One obstacle to the application of lncRNA findings from the la-boratory in the clinic lies in the rapid sequence evolution of these molecules, which results in highly varied nucleotide sequences among species [37]. However, H19 is known to be highly conserved between mice and humans, facilitating its use as a promising diagnostic bio-marker and therapeutic target [38,39]. In addition, we concluded from our study and a number of previous works that the re-expression of H19 in vessels, whether during tumor neovascular formation or in other blood vessels, may indicate a sort of vascular inflammatory disorder, such as the H19 re-expression observed in VSMCs from injured carotid arteries, VSMCs and endothelial cells from atherosclerotic arteries, and aortas from hyperhomocysteinemic mice [13,28,40]. It is thus tempting to propose that H19 is a sensitive and broad-spectrum indicator of vascular inflammatory disorders [13,40]. LncRNAs regulate gene ex-pression mostly transcriptionally and epigenetically, and less often translationally, as they are found relatively upstream within in-tracellular signaling networks [41–43]. Additionally, as an RNA struc-ture may be deployed more quickly and easily than proteins [44], the use of RNA as a mediator would rapidly alter regulatory functions without the need for protein translation [45]. These characteristics highlight the potential of lncRNAs as advantageous targets for rational ncRNA-based manipulation that is more rapid and economical than methods that rely on a protein-intervention system. Thus, it is reason-able for us to expect the manipulation of H19 to be feasible in future endeavors against AAA progression.

Some limitations of our study should be noted. First, our experiment adopted virus-mediated H19 interventions but not genetic modifica-tion-based methods. However, given that murine transgenic H19 overexpression is lethal during gestation, the utilization of this genetic method in H19 intervention is constricted [46]. In this work, luciferase activity analysis confirmed highly efficient and stable virus-mediated aortic H19 expression, and H19 intervention should thus be considered valid. Second, we observed re-expressed H19 in both aortic VSMCs and infiltrating macrophages, but whether and how H19 affects AAA for-mation through these cells were not studied and warrant future in-vestigation. In an injured carotid artery model, H19 re-expression was associated with SMC dedifferentiation, or so-called SMC phenotypic switching [40]. As phenotypically altered SMCs secrete inflammatory molecules, this observation might partially explain the source of these molecules. Third, our study concentrated on the H19/let-7a pathway in AAA; nonetheless, as lncRNAs have theoretical potency in regulating intracellular signaling networks, it remains to be explored whether there are other potential downstream targets of H19. In this context, a real-world therapeutic strategy based on H19 manipulation still awaits comprehensive and deeper study.

In summary, our work identified lncRNA H19 as a participant in AAA formation by intensifying aortic IL-6 and MCP-1 levels and mac-rophage infiltration. This IL-6-promoting effect is induced in part by an H19/let-7a ceRNA mechanism. These findings enrich our under-standing of lncRNA function during AAA pathogenesis and suggest the potential of lncRNA H19 as a novel therapeutic target in future drug design studies for AAA treatment.

Declarations of conflicts of interest

None.

Acknowledgments

Funding source

Appendix A. Supplementary data

Supplementary data to this article can be found online at https://doi.org/10.1016/j.yjmcc.2019.04.004.

References

[1] J. Golledge, P.E. Norman, Current status of medical management for abdominal aortic aneurysm, Atherosclerosis 217 (1) (2011) 57–63.

[2] K. Shimizu, R.N. Mitchell, P. Libby, Inflammation and cellular immune responses in abdominal aortic aneurysms, Arterioscler. Thromb. Vasc. Biol. 26 (5) (2006) 987–994.

[3] J. Juvonen, H.M. Surcel, J. Satta, A.M. Teppo, A. Bloigu, H. Syrjala, J. Airaksinen, M. Leinonen, P. Saikku, T. Juvonen, Elevated circulating levels of inflammatory cytokines in patients with abdominal aortic aneurysm, Arterioscler. Thromb. Vasc. Biol. 17 (11) (1997) 2843–2847.

[4] V. Treska, O. Topolcan, L. Pecen, Cytokines as plasma markers of abdominal aortic aneurysm, Clin. Chem. Lab. Med. 38 (11) (2000) 1161–1164.

[5] T. Saito, Y. Hasegawa, Y. Ishigaki, T. Yamada, J. Gao, J. Imai, K. Uno, K. Kaneko, T. Ogihara, T. Shimosawa, T. Asano, T. Fujita, Y. Oka, H. Katagiri, Importance of endothelial NF-kappaB signalling in vascular remodelling and aortic aneurysm formation, Cardiovasc. Res. 97 (1) (2013) 106–114.

[6] T.R. Mercer, M.E. Dinger, J.S. Mattick, Long non-coding RNAs: insights into functions, Nat. Rev. Genet. 10 (3) (2009) 155–159.

[7] X. Li, J. Zhou, K. Huang, Inhibition of the lncRNA Mirt1 attenuates acute myocardial infarction by suppressing NF-kappaB activation, Cell. Physiol. Biochem. 42 (3) (2017) 1153–1164.

[8] K. Shan, Q. Jiang, X.Q. Wang, Y.N. Wang, H. Yang, M.D. Yao, C. Liu, X.M. Li, J. Yao, B. Liu, Y.Y. Zhang, Y. J, B. Yan, Role of long non-coding RNA-RNCR3 in atherosclerosis-related vascular dysfunction, Cell Death Dis. 7 (6) (2016) e2248.

[9] Y. Han, J. Ma, J. Wang, L. Wang, Silencing of H19 inhibits the adipogenesis and inflammation response in ox-LDL-treated Raw264.7 cells by up-regulating miR-130b, Mol. Immunol. 93 (2018) 107–114.

[10] J.H. Lindeman, H. Abdul-Hussien, A.F. Schaapherder, J.H. Van Bockel, J.H. Von der Thusen, D.L. Roelen, R. Kleemann, Enhanced expression and activation of pro-inflammatory transcription factors distinguish aneurysmal from atherosclerotic aorta: IL-6- and IL-8-dominated inflammatory responses prevail in the human aneurysm, Clin. Sci. (Lond.) 114 (11) (2008) 687–697.

[11] J.X. Pan, LncRNA H19 promotes atherosclerosis by regulating MAPK and NF-kB signaling pathway, Eur. Rev. Med. Pharmacol. Sci. 21 (2) (2017) 322–328.

[12] W.T. Wang, H. Ye, P.P. Wei, B.W. Han, B. He, Z.H. Chen, Y.Q. Chen, LncRNAs H19 and HULC, activated by oxidative stress, promote cell migration and invasion in cholangiocarcinoma through a ceRNA manner, J. Hematol. Oncol. 9 (1) (2016) 117.

[13] A.M. Devlin, T. Bottiglieri, F.E. Domann, S.R. Lentz, Tissue-specific changes in H19 methylation and expression in mice with hyperhomocysteinemia, J. Biol. Chem. 280 (27) (2005) 25506–25511.

[14] D.Y. Li, A. Busch, H. Jin, E. Chernogubova, J. Pelisek, J. Karlsson, B. Sennblad, S. Liu, S. Lao, P. Hofmann, A. Backlund, S.M. Eken, J. Roy, P. Eriksson, B. Dacken, D. Ramanujam, A. Dueck, S. Engelhardt, R.A. Boon, H.H. Eckstein, J.M. Spin, P.S. Tsao, L. Maegdefessel, H19 induces abdominal aortic aneurysm development and progression, Circulation. 138 (15) (2018) 1551–1568.

[15] D.B. Trivedi, C.D. Loftin, J. Clark, P. Myers, L.M. DeGraff, J. Cheng, D.C. Zeldin, R. Langenbach, Beta-Arrestin2 deficiency attenuates abdominal aortic aneurysm formation in mice, Circ. Res. 112 (9) (2013) 1219–1229.

[16] G.M. Longo, W. Xiong, T.C. Greiner, Y. Zhao, N. Fiotti, B.T. Baxter, Matrix metalloproteinases 2 and 9 work in concert to produce aortic aneurysms, J. Clin. Invest. 110 (5) (2002) 625–632.

[17] G.L.T. Vieira, A.C. Lossie, D.C. Lay Jr., J.S. Radcliffe, J.P. Garner, Preventing, treating, and predicting barbering: a fundamental role for biomarkers of oxidative stress in a mouse model of trichotillomania, PLoS One 12 (4) (2017) e0175222.

[18] Y. Wang, H. Ait-Oufella, O. Herbin, P. Bonnin, B. Ramkhelawon, S. Taleb, J. Huang, G. Offenstadt, C. Combadiere, L. Renia, J.L. Johnson, P.L. Tharaux, A. Tedgui, Z. Mallat, TGF-beta activity protects against inflammatory aortic aneurysm progression and complications in angiotensin II-infused mice, J. Clin. Invest. 120 (2) (2010) 422–432.

[19] K. Satoh, P. Nigro, T. Matoba, M.R. O'Dell, Z. Cui, X. Shi, A. Mohan, C. Yan, J. Abe, K.A. Illig, B.C. Berk, Cyclophilin A enhances vascular oxidative stress and the development of angiotensin II-induced aortic aneurysms, Nat. Med. 15 (6) (2009) 649–656.

[20] B. Bostick, A. Ghosh, Y. Yue, C. Long, D. Duan, Systemic AAV-9 transduction in mice is influenced by animal age but not by the route of administration, Gene Ther. 14 (22) (2007) 1605–1609.

[21] S. Guo, S. Shen, J. Wang, H. Wang, M. Li, Y. Liu, F. Hou, Y. Liao, J. Bin, Detection of high-risk atherosclerotic plaques with ultrasound molecular imaging of glycoprotein IIb/IIIa receptor on activated platelets, Theranostics 5 (4) (2015) 418–430.

[22] Y. Chen, C. Zhang, S. Shen, S. Guo, L. Zhong, X. Li, G. Chen, G. Chen, X. He, C. Huang, N. He, W. Liao, Y. Liao, J. Bin, Ultrasound-targeted microbubble destruction enhances delayed BMC delivery and attenuates post-infarction cardiac remodeling by inducing engraftment signals, Clin. Sci. (Lond.) 130 (23) (2016) 2105–2120.

[23] C.W. Kim, S. Kumar, D.J. Son, I.H. Jang, K.K. Griendling, H. Jo, Prevention of abdominal aortic aneurysm by anti-microRNA-712 or anti-microRNA-205 in angiotensin II-infused mice, Arterioscler. Thromb. Vasc. Biol. 34 (7) (2014) 1412–1421.

[24] X.H. Zhu, Y.X. Yuan, S.L. Rao, P. Wang, LncRNA MIAT enhances cardiac hypertrophy partly through sponging miR-150, Eur. Rev. Med. Pharmacol. Sci. 20 (17) (2016) 3653–3660.

[25] C. Song, J. Zhang, Y. Liu, H. Pan, H.P. Qi, Y.G. Cao, J.M. Zhao, S. Li, J. Guo, H.L. Sun, C.Q. Li, Construction and analysis of cardiac hypertrophy-associated lncRNA-mRNA network based on competitive endogenous RNA reveal functional lncRNAs in cardiac hypertrophy, Oncotarget 7 (10) (2016) 10827–10840.

[26] X. Li, X. He, H. Wang, M. Li, S. Huang, G. Chen, Y. Jing, S. Wang, Y. Chen, W. Liao, Y. Liao, J. Bin, Loss of AZIN2 splice variant facilitates endogenous cardiac regeneration, Cardiovasc. Res. 114 (12) (2018) 1642–1655.

[27] S. Ounzain, R. Micheletti, T. Beckmann, B. Schroen, M. Alexanian, I. Pezzuto, S. Crippa, M. Nemir, A. Sarre, R. Johnson, J. Dauvillier, F. Burdet, M. Ibberson, R. Guigo, I. Xenarios, S. Heymans, T. Pedrazzini, Genome-wide profiling of the cardiac transcriptome after myocardial infarction identifies novel heart-specific long non-coding RNAs, Eur. Heart J. 36 (6) (2015) (353-68a).

[28] L. Zhang, H. Cheng, Y. Yue, S. Li, D. Zhang, R. He, H19 knockdown suppresses proliferation and induces apoptosis by regulating miR-148b/WNT/beta-catenin in ox-LDL-stimulated vascular smooth muscle cells, J. Biomed. Sci. 25 (1) (2018) 11.

[29] K.G. Jones, D.J. Brull, L.C. Brown, M. Sian, R.M. Greenhalgh, S.E. Humphries, J.T. Powell, Interleukin-6 (IL-6) and the prognosis of abdominal aortic aneurysms, Circulation 103 (18) (2001) 2260–2265.

[30] B.L. Cheuk, S.W. Cheng, Can local secretion of prostaglandin E2, thromboxane B2, and interleukin-6 play a role in ruptured abdominal aortic aneurysm? World J. Surg. 32 (1) (2008) 55–61.

[31] J. Dawson, G.W. Cockerill, E. Choke, A.M. Belli, I. Loftus, M.M. Thompson, Aortic aneurysms secrete interleukin-6 into the circulation, J. Vasc. Surg. 45 (2) (2007) 350–356.

[32] A.K. Sharma, G. Lu, A. Jester, W.F. Johnston, Y. Zhao, V.A. Hajzus, M.R. Saadatzadeh, G. Su, C.M. Bhamidipati, G.S. Mehta, I.L. Kron, V.E. Laubach, M.P. Murphy, G. Ailawadi, G.R. Upchurch Jr., Experimental abdominal aortic aneurysm formation is mediated by IL-17 and attenuated by mesenchymal stem cell treatment, Circulation 126 (11 Suppl 1) (2012) S38–S45.

[33] S.C. Harrison, A.J. Smith, G.T. Jones, D.I. Swerdlow, R. Rampuri, M.J. Bown, L. Folkersen, A.F. Baas, G.J. de Borst, J.D. Blankensteijn, J.F. Price, Y. van der Graaf, S. McLachlan, O. Agu, A. Hofman, A.G. Uitterlinden, A. Franco-Cereceda, Y.M. Ruigrok, F.N. van't Hof, J.T. Powell, A.M. van Rij, J.P. Casas, P. Eriksson, M.V. Holmes, F.W. Asselbergs, A.D. Hingorani, S.E. Humphries, Interleukin-6 receptor pathways in abdominal aortic aneurysm, Eur. Heart J. 34 (48) (2013) 3707–3716.

[34] K. Yoshimura, H. Aoki, Y. Ikeda, K. Fujii, N. Akiyama, A. Furutani, Y. Hoshii, N. Tanaka, R. Ricci, T. Ishihara, K. Esato, K. Hamano, M. Matsuzaki, Regression of abdominal aortic aneurysm by inhibition of c-Jun N-terminal kinase, Nat. Med. 11 (12) (2005) 1330–1338.

[35] M.S. Ebert, P.A. Sharp, Emerging roles for natural microRNA sponges, Curr. Biol. 20 (19) (2010) R858–R861.

[36] L. Salmena, L. Poliseno, Y. Tay, L. Kats, P.P. Pandolfi, A ceRNA hypothesis: the Rosetta Stone of a hidden RNA language? Cell 146 (3) (2011) 353–358.

[37] A. Necsulea, M. Soumillon, M. Warnefors, A. Liechti, T. Daish, U. Zeller, J.C. Baker, F. Grutzner, H. Kaessmann, The evolution of lncRNA repertoires and expression patterns in tetrapods, Nature 505 (7485) (2014) 635–640.

[38] K. Ishihara, H. Sasaki, An evolutionarily conserved putative insulator element near the 3′ boundary of the imprinted Igf2/H19 domain, Hum. Mol. Genet. 11 (14) (2002) 1627–1636.

[39] M. Paulsen, S. Takada, N.A. Youngson, M. Benchaib, C. Charlier, K. Segers, M. Georges, A.C. Ferguson-Smith, Comparative sequence analysis of the imprinted Dlk1-Gtl2 locus in three mammalian species reveals highly conserved genomic elements and refines comparison with the Igf2-H19 region, Genome Res. 11 (12) (2001) 2085–2094.

[40] D.K. Kim, L. Zhang, V.J. Dzau, R.E. Pratt, H19, a developmentally regulated gene, is reexpressed in rat vascular smooth muscle cells after injury, J. Clin. Invest. 93 (1) (1994) 355–360.

[41] Y.M. Li, G. Franklin, H.M. Cui, K. Svensson, X.B. He, G. Adam, R. Ohlsson, S. Pfeifer, The H19 transcript is associated with polysomes and may regulate IGF2 expression in trans, J. Biol. Chem. 273 (43) (1998) 28247–28252.

[42] F. Wilkin, J. Paquette, E. Ledru, C. Hamelin, M. Pollak, C.L. Deal, H19 sense and antisense transgenes modify insulin-like growth factor-II mRNA levels, Eur. J. Biochem. 267 (13) (2000) 4020–4027.

[43] S. Lottin, A.S. Vercoutter-Edouart, E. Adriaenssens, X. Czeszak, J. Lemoine, M. Roudbaraki, J. Coll, H. Hondermarck, T. Dugimont, J.J. Curgy, Thioredoxin post-transcriptional regulation by H19 provides a new function to mRNA-like noncoding RNA, Oncogene 21 (10) (2002) 1625–1631.

[44] P.J. Batista, H.Y. Chang, Long noncoding RNAs: cellular address codes in development and disease, Cell 152 (6) (2013) 1298–1307.

[45] M.D. Ballantyne, R.A. McDonald, A.H. Baker, lncRNA/MicroRNA interactions in the vasculature, Clin. Pharmacol. Ther. 99 (5) (2016) 494–501.

[46] M.E. Brunkow, S.M. Tilghman, Ectopic expression of the H19 gene in mice causes prenatal lethality, Genes Dev. 5 (6) (1991) 1092–1101.